This article was downloaded by: *[Canadian Research Knowledge Network]*
On: *1 June 2010*
Access details: *Access Details: [subscription number 918588849]*
Publisher *Taylor & Francis*
Informa Ltd Registered in England and Wales Registered Number: 1072954 Registered office: Mortimer House, 37-41 Mortimer Street, London W1T 3JH, UK

Combustion Science and Technology
Publication details, including instructions for authors and subscription information:
http://www.informaworld.com/smpp/title~content=t713456315

Dynamics of Lean-Premixed Turbulent Combustion at High Turbulence Intensities

Frank T. C. Yuen[a]; Ömer L. Gülder[a]
[a] Institute for Aerospace Studies, University of Toronto, Ontario, Canada

Online publication date: 01 June 2010

To cite this Article Yuen, Frank T. C. and Gülder, Ömer L.(2010) 'Dynamics of Lean-Premixed Turbulent Combustion at High Turbulence Intensities', Combustion Science and Technology, 182: 4, 544 — 558
To link to this Article: DOI: 10.1080/00102200903463274
URL: http://dx.doi.org/10.1080/00102200903463274

PLEASE SCROLL DOWN FOR ARTICLE

Full terms and conditions of use: http://www.informaworld.com/terms-and-conditions-of-access.pdf

This article may be used for research, teaching and private study purposes. Any substantial or systematic reproduction, re-distribution, re-selling, loan or sub-licensing, systematic supply or distribution in any form to anyone is expressly forbidden.

The publisher does not give any warranty express or implied or make any representation that the contents will be complete or accurate or up to date. The accuracy of any instructions, formulae and drug doses should be independently verified with primary sources. The publisher shall not be liable for any loss, actions, claims, proceedings, demand or costs or damages whatsoever or howsoever caused arising directly or indirectly in connection with or arising out of the use of this material.

Combust. Sci. and Tech., 182: 544–558, 2010
Copyright © Taylor & Francis Group, LLC
ISSN: 0010-2202 print/1563-521X online
DOI: 10.1080/00102200903463274

Taylor & Francis
Taylor & Francis Group

Downloaded By: [Canadian Research Knowledge Network] At: 17:52 1 June 2010

DYNAMICS OF LEAN-PREMIXED TURBULENT COMBUSTION AT HIGH TURBULENCE INTENSITIES

Frank T. C. Yuen and Ömer L. Gülder
Institute for Aerospace Studies, University of Toronto, Ontario, Canada

Premixed turbulent flames of methane-air stabilized on a Bunsen-type burner were studied to investigate the structure of the flame front at a wide range of turbulence intensities. The nondimensional turbulence rms velocity, rms velocity divided by the laminar flame speed, covered the range from about 3 to 24. The equivalence ratio was varied from 0.6 to stoichiometric. The flame front data were obtained using planar Rayleigh imaging, and particle image velocimetry was used to measure instantaneous velocity field for the experimental conditions studied. Flame front thickness increased slightly with increasing nondimensional turbulence rms velocity. There was no significant difference in flame thickening whether the flame thickness was evaluated at progress variable 0.5, corresponding to the reaction zone, or 0.3, corresponding to the preheat zone. Flame front curvature decreased with increasing turbulence rms velocity. Flame front curvature statistics displayed a Gaussian-like distribution, which centered about zero for all the flame conditions studied during the investigation. Flame surface densities evaluated from flame front images showed almost no dependence on the nondimensional turbulence intensity. Flame surface densities integrated over the flame brush volume also did not show any sensitivity to the nondimensional turbulence rms velocity. This was discussed in the framework of a flame surface density-based turbulent premixed flame propagation closure model. The implication is that the conceptual increase in flame surface density with turbulence may not be the dominant mechanism for flame velocity enhancement in turbulent combustion in the region specified as the flamelet combustion regime by the current turbulent premixed combustion diagrams. Further, the applicability of the flamelet approach may be limited to a much smaller range of conditions than presently believed.

Keywords: Flame surface curvature; Flame surface density; Flamelet regimes; Turbulent premixed combustion

INTRODUCTION

The flamelet assumption has been widely used to model the complex coupling between chemistry and heat and mass transfer. The flamelet model assumes that the reactants and products are separated by thin reacting interfaces that preserve their locally laminar structure. These thin reacting interfaces are called flamelets and in most formulations are taken to be a passive surface. The main function of the turbulent field is to wrinkle and strain this passive surface. Then at high Damköhler

Received 2 March 2009; revised 5 October 2009; accepted 12 October 2009.
Address correspondence to Ömer L. Gülder, Institute for Aerospace Studies, University of Toronto, 4925 Dufferin Street, Toronto, Ontario M3H 5T6, Canada. E-mail: ogulder@utias.utoronto.ca

numbers, a premixed flame front can be taken as consisting of regions of reactants and products separated by thin laminar flamelets. Because the instantaneous behavior of these thin layers is the same as those of laminar flames, turbulent burning velocity can be approximated by the product of the flamelets surface area and laminar burning velocity corrected for the effect of stretch and flame curvature. However, more recent experimental work has presented evidence that suggests the passive characteristics of the premixed flamelets and their laminar thermal structure may not be preserved beyond medium turbulence intensities (Gülder et al., 2000; Hartung et al., 2008), and the scalar gradients within the flame front are destroyed by turbulence (Hartung et al., 2008). Similarly, experimental measurements of flame surface densities have indicated that the flame surface area is not the dominant factor in increasing the turbulent burning velocity under the conditions corresponding to the flamelet regimes (Chen & Bilger, 2002; Cintosun et al., 2007; Gülder, 2007; Gülder & Smallwood, 2007; Gülder et al., 2000).

The most recent regime diagram for the premixed turbulent combustion (Peters, 2000) extends the traditional flamelet regime (i.e., wrinkled and corrugated flamelets regions) further up to $\mathrm{Ka} = 100$ from the previous upper limit of $\mathrm{Ka} = 1$, where the Karlovitz number, Ka, is defined as the ratio of chemical time scale to the Kolmogorov time scale. The region between $\mathrm{Ka} = 1$ and $\mathrm{Ka} = 100$ is called the thin reaction zones, and the similar flamelet assumptions are claimed to be still valid (Peters, 2000). In the theory for the thin reaction zones regime the propagation speed of the instantaneous flame is given by $s_\kappa = D\kappa$, where D is the diffusivity and κ is the local flame curvature. It is argued that this value is much higher than the laminar burning velocity in this regime.

The objectives of this study were to evaluate flame front temperature profiles and their temperature gradients, thermal flame front thickness, flame curvature statistics, and flame surface density. These evaluations provide means to understand the interaction between turbulence field characteristics and flame front dynamics as well as the effect of turbulence and curvature on the flame front structure. The results are discussed in relation to the validity range of the flamelet models for various flame conditions.

EXPERIMENTAL METHOD

Premixed turbulent conical flames were produced by an axisymmetric Bunsen-type burner with an inner nozzle diameter of 11.2 mm. Premixed turbulent methane-air flames with equivalence ratios from 0.6 to 1.0 were stabilized by using an annular pilot flame. A premixed methane-air flame is used for low turbulence intensities; at higher turbulence levels an ethylene-air flame was used as the annular pilot. Perforated plates positioned three nozzle diameters upstream of the burner rim controlled the turbulence levels.

Particle image velocimetry (PIV) was used to measure instantaneous velocity field for the experimental conditions studied. Summary of experimental conditions for all flames studied are tabulated in Table 1. The PIV experiment was conducted separately from the Rayleigh scattering experiments. The system consisted of a double-pulsed second harmonic (532 nm) Nd:YAG laser working at an energy level of 50 mJ/pulse and a frequency of 15 Hz; a CCD camera with an array size of

Downloaded By: [Canadian Research Knowledge Network] At: 17:52 1 June 2010

Table 1 Summary of experimental conditions. Φ is fuel–air equivalence ratio; Λ, λ, and η are integral, Taylor and Kolmogorov length scales, respectively; u'/S_L is nondimensional turbulence rms velocity; δ_L^o is the unperturbed laminar flame thickness calculated by detailed kinetics (H. K. Moffat & D. Goodwin, 2005); Re_Λ is the Reynolds number based on u' and integral length scale Λ; Ka is the Karlovitz number; and D is the molecular diffusivity calculated at 1800 K

Flame number	Φ	Λ (mm)	λ (mm)	η (mm)	u'/S_L	δ_L^o (mm)	Re_Λ	Ka	D (cm^2/s)
M1	1.0	1.62	0.45	0.052	3.2	0.45	98	1.1	
M2	0.9	1.62	0.45	0.052	3.7	0.48	97	1.4	
M3	0.8	1.62	0.45	0.052	4.7	0.54	97	2.2	
M4	0.7	1.62	0.45	0.052	6.4	0.68	97	4.2	
M5	0.6	1.62	0.45	0.052	10.8	1.0	96	11.9	2.96
M6	1.0	1.64	0.44	0.052	3.3	0.45	101	1.1	
M7	0.9	1.64	0.44	0.052	3.7	0.48	100	1.4	
M8	0.8	1.64	0.44	0.052	4.7	0.54	100	2.2	
M9	0.7	1.64	0.44	0.052	6.6	0.68	100	4.3	
M10	0.6	1.64	0.44	0.052	11.0	1.0	99	12.1	2.96
M11	1.0	1.79	0.46	0.029	7.3	0.45	242	3.4	
M12	0.9	1.79	0.46	0.029	8.2	0.48	241	4.3	3.37
M13	0.8	1.79	0.46	0.029	10.4	0.54	240	7.0	3.32
M14	0.7	1.79	0.46	0.029	14.4	0.68	239	13.4	3.26
M15	0.6	1.79	0.46	0.029	24.1	1.0	239	37.7	2.96

Downloaded By: [Canadian Research Knowledge Network] At: 17:52 1 June 2010

1600×1186 pixels and equipped with a 2.8 f-number 60 mm focal length camera objective. This optical setup was used to capture the flow condition above the nozzle exit with a view area of 15.7 mm × 11.6 mm and a resolution of 9.8 μm/pixel. The time separation between the two laser pulses was 10 μs. The submicron oil droplets were generated by a nebulizer as seeding particles. The image scale factor was 1.326, the interrogation region was 32×32 pixels, and the pixel pitch was 5.56 μm. The multiplication of these terms gives the actual PIV resolution, which is about 0.24 mm. This is the smallest velocity structure that can be resolved, which is smaller than the Taylor length scales in Table 1. The length scales were estimated by using the velocity field data from the PIV measurements, which yielded fluctuating rms velocity u'. The auto-correlation functions of u' were calculated along the length of the image. The integral length scales were found by integrating the auto-correlation functions to where they first crossed zero. The Taylor length scales were estimated by constructing an osculating parabola for the auto-correlation function. The distance to which the parabola crosses zero is the Taylor length scale.

Flame front images were captured using planar Rayleigh scattering (Eckbreth, 1996; Dibble & Hollenbach, 1981; Miles et al., 2001). This setup consisted of a third harmonic (355 nm) Nd:YAG laser working at an energy level of 305 mJ/pulse and a frequency of 10 Hz; a set of beam-shaping optics through which the laser beam passed to produce a laser sheet of 60 mm high and 150 μm thick; an intensified CCD camera with an array size of 1024×1280 pixels positioned at 90° to the scattered light, and equipped with a 4.1 f-number 94 mm focal length camera objective. With this setup, a capture area of 57 mm × 46 mm and a resolution of 45 μm/pixel were achieved. The signal to noise ratio for the products was about 14.3, and for the reactants was 23.8. This was found by calculating the ratio between the mean

and standard deviation for an area of 2500 pixels in the product and reaction regions of the flame. Typical Rayleigh scattering intensity is about 260 counts for reactant pixels and 72 for product pixels. However, with this arrangement of the optical layout, it was necessary to divide the flame into three sections along the flame centerline, and images were captured for three sections separately. Each section of the flame had a height of 44 mm and width of 22 mm. The centers of the sections were 66.5, 96.5, and 121.5 mm above the burner rim; these sections were referred as *low, middle*, and *top* sections of the flame, respectively, in the Results and Discussion section of the paper. More than 300 images were captured for each experimental condition.

Rayleigh scattering images were first processed using a 3×3 nonlinear sliding average filter to reduce noise in the raw images. The total number density of the molecules was directly proportional to temperature by using the ideal gas law and assuming constant pressure conditions. The raw Rayleigh scattering density images were then converted into temperature field using the following expression (Sinibaldi et al., 1998; Soika et al., 1998),

$$T_{\text{flame}} = \underbrace{\frac{\left(\sum_i \sigma_i \chi_i\right)_{\text{mix}}}{\left(\sum_i \sigma_i \chi_i\right)_{\text{air}}}}_{k} T_{\text{air}} \underbrace{\frac{(I_{\text{air}} - I_{\text{back}})}{(I_{\text{flame}} - I_{\text{back}})}}_{I} \tag{1}$$

where T_{flame} is calculated for each pixel in each image, σ_i is the Rayleigh scattering cross-section for each molecule i, χ_i is the mole fraction of different species, and I_{flame} and I_{air} are the Rayleigh scattering signal intensities of the flame and a calibration image with air at temperature T_{air}. I_{back} is the background signal intensity, which consisted of the dark noise of the intensified CCD camera, the laboratory background light, and laser reflections. Due to its parasitic nature in the experimental setup, I_{back} was estimated by setting the flame temperature to that of the adiabatic flame and solving Eq. (1) in the product region of the each flame image. I_{back} for each image was calculated so that the flame temperature in the product region was equivalent to adiabatic flame temperature (Knaus et al., 2005). The background signal was approximately 26 counts and the variation was less than ± 3 counts throughout the flame image. So it was reasonable to use a single background count for the entire image.

The Rayleigh scattering cross sections that have been tabulated in (Sutton & Driscoll, 2004) were used. The variation of the different combustion species across flame front was obtained through a 1-D laminar flame simulation with the Cantera package, which uses the GRI-3.0 mechanism (Moffat & Goodwin, 2005). From these data, the variations of the effective Rayleigh scattering cross sections (k, first fraction on the right hand side of Eq. [1]) with temperature were calculated for methane and propane flames. The peaks of the probability density functions of the intensity ratio (I, last fraction on the right hand side of Eq. [1]) that correspond to the burnt and unburned gases were determined. These peak intensity ratio values were then related to the burnt and unburned gas temperatures. In this way, relationships of k versus I were established for different equivalence ratios and fuels. So for each I value, there was a corresponding k value for calculating the flame temperature at each pixel. A set of instantaneous Rayleigh scattering temperature images of methane flames are shown in Figure 1 at various nondimensional turbulence rms velocities.

Downloaded By: [Canadian Research Knowledge Network] At: 17:52 1 June 2010

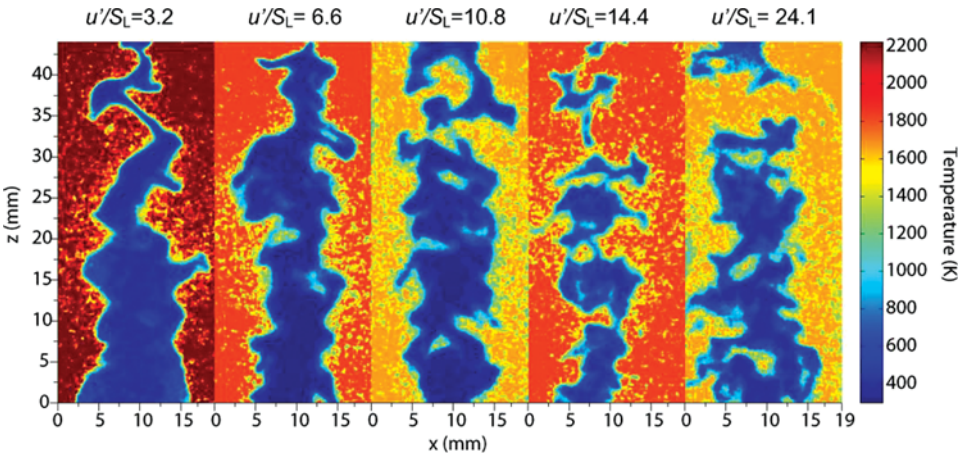

Figure 1 Instantaneous Rayleigh images at different turbulent intensities in methane flames. u' is the rms velocity and S_L is the laminar burning velocity.

The maximum resolution of the Rayleigh imaging system was found using the Contrast Transfer Function (CTF), which corresponds to 22 line-pairs/mm at CTF of 10%. Thus, the limiting resolution for the Rayleigh scattering measurements would be the laser sheet thickness, which is 150 μm. The Rayleigh scattering images were processed to provide instantaneous temperature gradients, ∇T, at progress variable $c = 0.5$ and 0.3, where $c = (T - T_u)/(T_b - T_u)$. T is the instantaneous temperature, T_b is the burnt gas temperature, set equal to the flame temperature calculated from Eq. (1), and T_u is the unburned gas temperature. Thicknesses were calculated using the following expression:

$$\delta_{th} = \frac{T_b - T_u}{|\nabla T|_{max}} \tag{2}$$

The term $|\nabla T|_{max}$ is the maximum temperature gradient along the direction normal to the flame front. The flame thickness evaluated at $c = 0.5$ can be considered as the characteristics of reaction zone thickness, whereas the one at $c = 0.3$ can be treated as the representative of preheat zone thickness (Dinkelacker, 1998; Soika et al., 1998). The c contours were found using an edge detection algorithm. Two-dimensional ∇T was extracted at each point along those contours. T_u and T_b were found from the probability density function of the temperature distribution of each image. Laminar thermal flame thicknesses (δ_L^0) were calculated from the temperature profiles across a 1-D laminar flame simulation. This was performed with the Cantera package, which uses the GRI-3.0 mechanism (Moffat & Goodwin, 2005).

Using the analysis method described by Wang and Clemens (2004), dissipation structures larger than laser sheet thickness of 150 μm were found to have a relative error of 9% in flame thickness and 8% relative error for temperature gradients. After the $c = 0.5$ contour was found, local curvature, κ, at each pixel point along the flame

Downloaded By: [Canadian Research Knowledge Network] At: 17:52 1 June 2010

contour was calculated using:

$$\kappa = \frac{\dot{x}\ddot{y} - \dot{y}\ddot{x}}{(\dot{x}^2 + \dot{y}^2)^{3/2}} \tag{3}$$

where $\dot{x} = \mathrm{d}x/\mathrm{d}s$ and $\ddot{x} = \mathrm{d}^2x/\mathrm{d}s^2$ are the first and second derivatives with respect to s, which is the flame contour length measured from a fixed origin on the flame front similar to the procedures used by Haq et al. (2002), Halter et al. (2005), and Chen (2007). The contours corresponding to $c = 0.5$ were filtered by a zero-phase digital filter that processed the contours in the forward and reverse directions. These provided no phase distortion and doubled the filter order. The filter length was chosen to be five points, which provided a filter order of eight. These filtered contours were then differentiated to give their respective first and second derivatives. The derivative curves were filtered again using the same filter and then curvatures were found using the Eq. (3). The minimum radius of curvature that can be resolved was found to be limited by the laser sheet thickness, which was 0.15 mm. The uncertainty in determining flame front curvature was about 25%. The diffusivities, D, are calculated at about 1800 K by using the Cantera package (Moffat & Goodwin, 2005) and assuming that the Schmidt number was unity.

Downloaded By: [Canadian Research Knowledge Network] At: 17:52 1 June 2010

RESULTS AND DISCUSSION

Flame front thicknesses evaluated from temperature gradients obtained from 2-D Rayleigh scattering measurements show a very mild sensitivity to nondimensional turbulence intensity, u'/S_L. The variation of the flame front thickness based on the temperature gradient at progress variable $c = 0.5$ and $c = 0.3$ with methane flames are shown in Figures 2 and 3, respectively. At all three sections of the flame, the flame front thickness seemed to increase slightly with nondimensional turbulence intensity. Flame front thickness values plotted in Figures 2 and 3 represent the most probable thicknesses taken as the peak values of the thickness probability density functions estimated from 2-D temperature gradients. At $c = 0.3$, the thickness was more related to the thickness of the preheat layer, whereas at $c = 0.5$ it was more related to the thickness of the reaction zone. These results indicate that the thickening process with increasing turbulence is more or less the same for both the reaction zone and the preheat zone for premixed turbulent methane flames, although the thickness change appears to be more prominent in the reaction zone. In a recent numerical simulation, however, it was found that the thickening process in the reaction zone is much weaker than that in the preheat zone (Kim & Pitsch, 2007). It was shown by De Goey et al. (2005) that measurements obtained by 2-D techniques are systematically higher than those measured by 3-D techniques by about 10–15% for premixed turbulent methane flames within the nondimensional turbulence rms intensity range of 5–19, and flame thickness measurement obtained by 2- and 3-D techniques show the same trend with the nondimensional turbulence rms intensity.

The probability density functions of methane flame surface curvatures for the middle section of the flames are shown in Figure 4 at various nondimensional turbulence intensities. Curvature pdfs display a Gaussian behavior at all turbulence

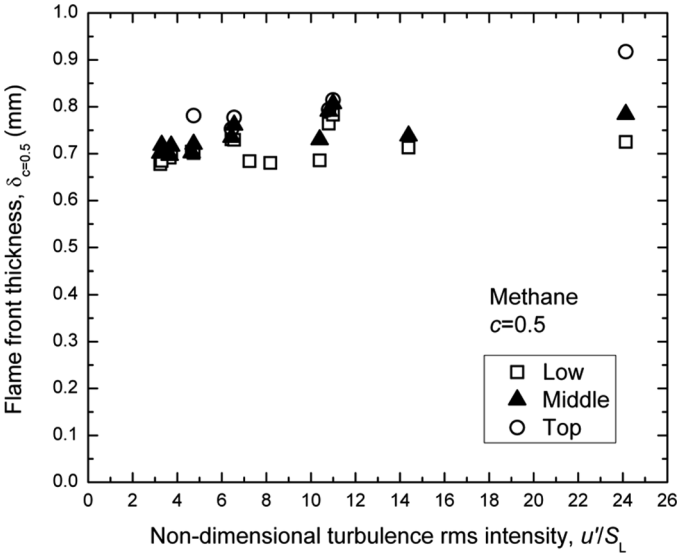

Figure 2 Variation of the peak reaction zone thickness evaluated at $c = 0.5$ as a function of nondimensional turbulence rms velocity.

intensities. Similar curvature pdfs were obtained with the bottom and top (Figure 5) sections of methane flames. Similar trends observed in Figures 4 and 5 were also reported by Haq et al. (2002) and Shepherd et al. (2002). A sample showing the variation of instantaneous curvatures along the flame contour for flames M1, M5,

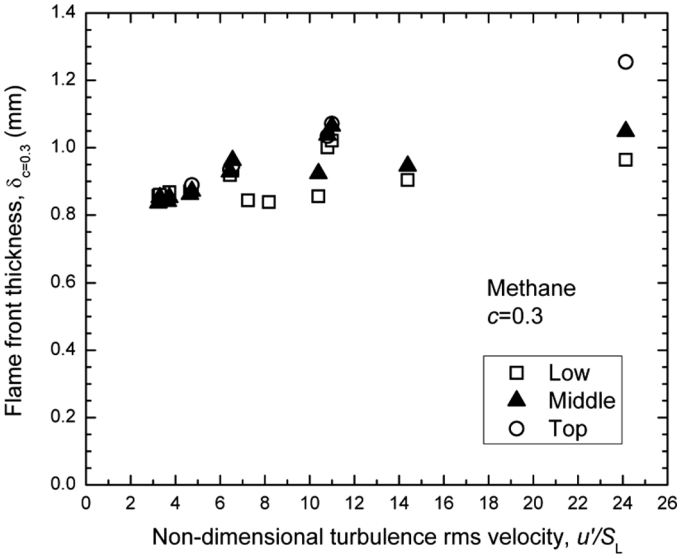

Figure 3 Variation of the peak preheat zone thickness evaluated at $c = 0.3$ as a function of nondimensional turbulence rms velocity.

Downloaded By: [Canadian Research Knowledge Network] At: 17:52 1 June 2010

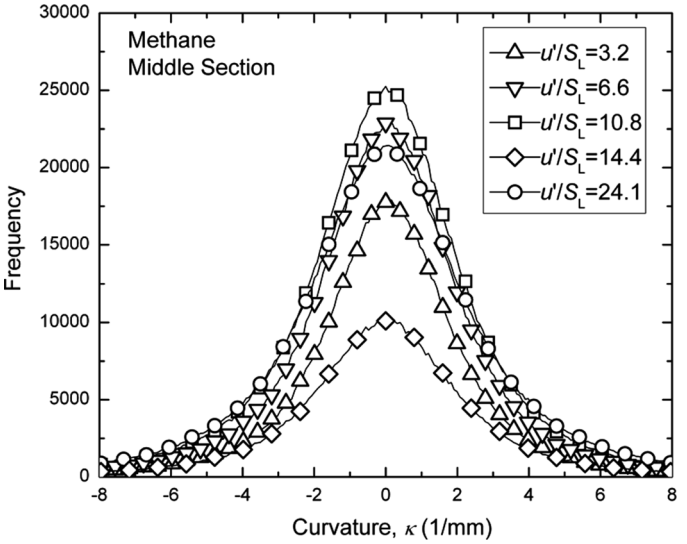

Figure 4 Probability density functions of methane flame curvatures at various nondimensional turbulence rms velocities at the middle section of the flame.

and M15 as a function of normalized path length s is shown in Figure 6. Local curvatures were observed to be more or less equally distributed among positive and negative curvature values.

To obtain flame surface densities, two different methods were used; the gradient of the progress variable c (Pope, 1988), and the method proposed by Shepherd

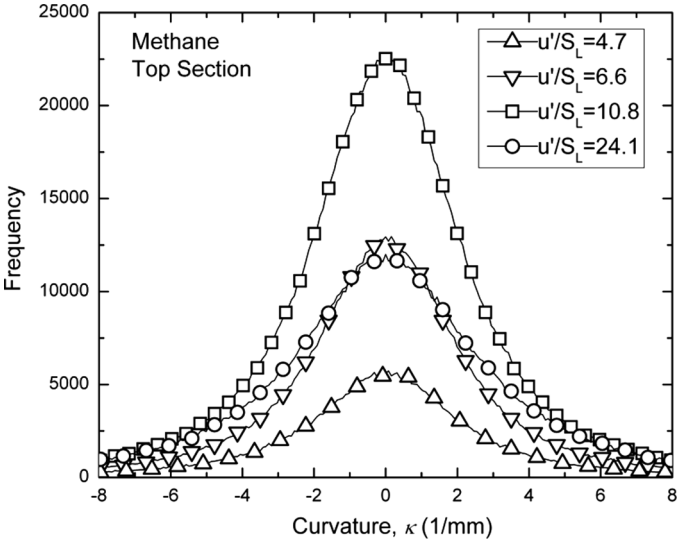

Figure 5 Probability density functions of methane flame curvatures at various nondimensional turbulence rms velocities at the top section of the flame.

Downloaded By: [Canadian Research Knowledge Network] At: 17:52 1 June 2010

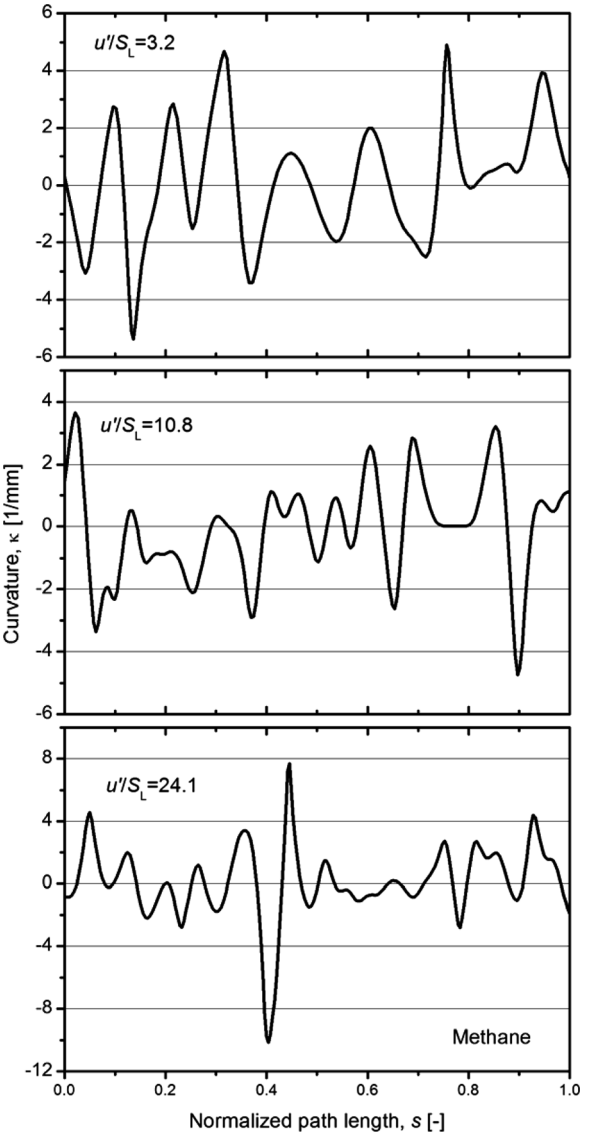

Figure 6 A sample of variation of instantaneous curvatures along the flame contour for the flames M1, M5, and M15 as a function of normalized path length *s*.

(1996). The flame surface density data evaluated as a function of nondimensional turbulence rms velocity using the gradient of the progress variable method are shown in Figure 7 for the middle section of the flames and in Figure 8 for the lower section of the flames. Flame surface density evaluated by using the method by Shepherd (1996) for the lower section of the flames is shown in Figure 9. In both methods, the flame surface density peaked around a value of the progress variable close to 0.5. The maximum values of the flame surface densities did not show any significant

Downloaded By: [Canadian Research Knowledge Network] At: 17:52 1 June 2010

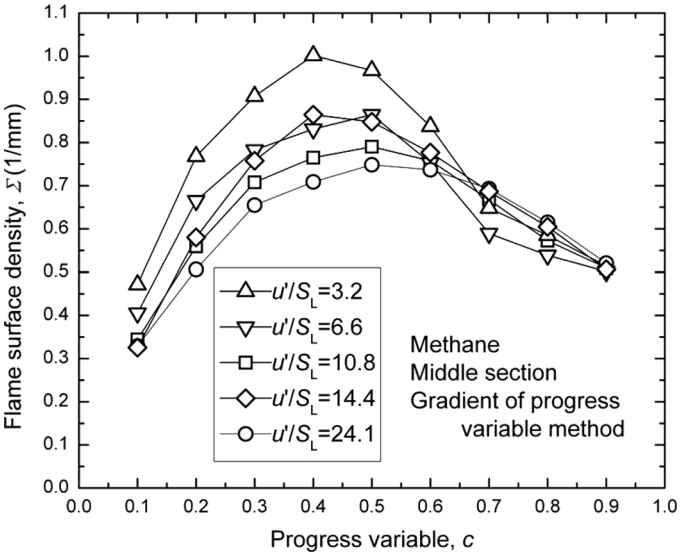

Figure 7 Flame surface density evaluated by the gradient of the progress variable (Pope, 1988) as a function of progress variable c (middle section of methane flames).

sensitivity to nondimensional turbulence rms velocity for both sections of the flames. The similar trend can be seen in the 3-D FSD measurements by Chen and Bilger (2002). It should be noted that the absolute values of the flame surface densities obtained using the method proposed by Shepherd (1996) are systematically higher

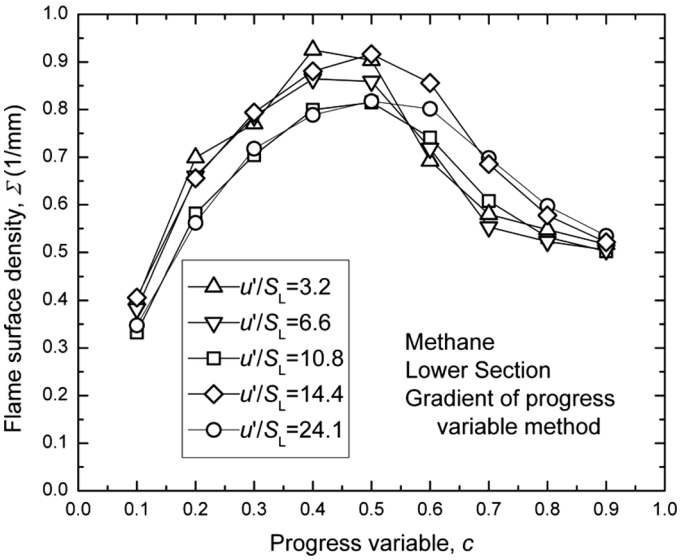

Figure 8 Flame surface density evaluated by the gradient of the progress variable (Pope, 1988) as a function of progress variable c (lower section of methane flames).

Downloaded By: [Canadian Research Knowledge Network] At: 17:52 1 June 2010

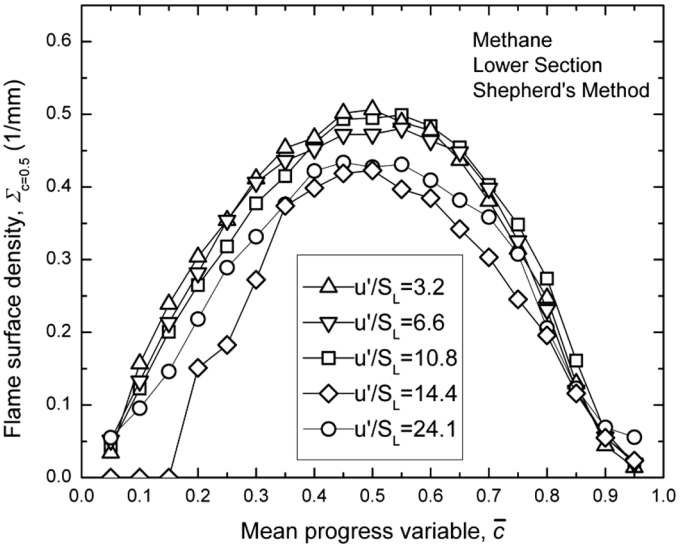

Figure 9 Flame surface density evaluated by the method proposed by Shepherd (1996) at $c = 0.5$ as a function of mean progress variable (lower section of methane flames).

than those evaluated by the gradient of the progress variable. The ratio of the two is about 2 (see Figures 8 and 9).

A 3-D estimate of flame surface density could be obtained from 2-D measurements by a correction using the individual flame front orientation angle. This angle was calculated by evaluating the gradient of mean progress variable in two directions in the plane of measurements, and determining the unit normal vectors in both directions. The mean direction cosine varied slightly, through the whole range of turbulence intensities, between 0.64 and 0.72, and most values were around 0.65. This is very close to the typical value for Bunsen flames of 0.7 reported by Deschamps et al. (1996) and the values of 0.55–0.65 reported by Chen and Bilger (2002). There were almost no changes in the direction cosine across the flame front. Shepherd and Ashurst (1992) showed that 2- and 3-D direction cosine pdfs are very similar and it is possible to estimate the true mean direction cosine from 2-D images. The present results have the same trend as reported in Shepherd and Ashurst's (1992) study.

It can be shown that the nondimensional turbulent burning velocity is proportional to the flame surface density integrated over the flame brush volume (see Gülder, 2007):

$$\frac{S_T}{S_L} = \frac{\int \Sigma \mathrm{d}V}{A_o} \tag{4}$$

The flame surface density data obtained in this study were used to evaluate the integrated flame surface densities for methane flames. Integrated flame surface densities are plotted, along with turbulent flame burning velocities determined experimentally, as a function of nondimensional turbulence rms velocity in Figure 10. Burning velocities were determined using the procedure outlined in

Downloaded By: [Canadian Research Knowledge Network] At: 17:52 1 June 2010

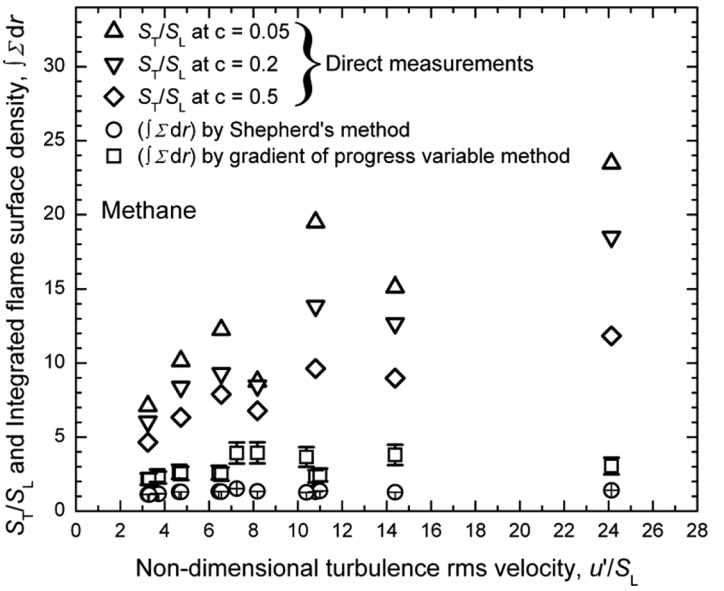

Figure 10 Variation of integrated flame surface density and nondimensional turbulent burning velocity of premixed turbulent methane flames with nondimensional turbulence rms velocity. Direct measurements refer to burning velocities determined using the procedure outlined in Gülder et al. (2000) and Gülder and Smallwood (2007). Error bars on integrated flame surface densities represent systematic and random errors and are about 15–20% (Yuen, 2009).

Gülder et al.'s (2000) and Gülder and Smallwood's (2007) studies. Integrated flame surface density shows no clear dependence on the turbulence intensity for the turbulent flame conditions studied in the present work. The observations that the integrated flame surface density do not change with the nondimensional turbulence intensity have some serious implications. Experimental measurements on turbulent premixed flames have shown that the turbulent burning velocity increases with increasing turbulence. Turbulent burning velocity data from the present measurements also show an increasing trend with increasing nondimensional turbulence rms velocity as shown in Figure 10. The turbulent burning velocity S_T increases as the turbulence intensity is increased. Thus, the integrated flame surface density is expected to increase with increasing u'/S_L in accordance with Eq. (4); however, it does not show any evidence of significant dependence on the flow turbulence. These results are similar to the ones reported by Smallwood and Gülder (2007) for propane flames.

Markstein (1964) formulated the level set equation for flame propagation that is now known as the *G*-equation:

$$\frac{\partial G}{\partial t} + v \cdot \nabla G = s_L |\nabla G| \tag{5}$$

Equation (5) was modified to represent the physics of the flame propagation within the thin reaction zones regime. In the theory for the thin reaction zones regime

Downloaded By: [Canadian Research Knowledge Network] At: 17:52 1 June 2010

(Peters, 2000) the propagation speed of the instantaneous flame is given by $s_\kappa = D\kappa$, where D is the diffusivity and κ is the local flame curvature. It is argued that this value is much higher than the laminar burning velocity in this regime. The proposal that s_κ should be used instead of the laminar burning velocity in the thin reaction zone regime is based on the two-dimensional direct numerical simulation (DNS) data (Peters et al., 1998). The proposed level set equation for the thin reaction zones regime is a modification of the G-equation, given as (Peters, 2000):

$$\frac{\partial G}{\partial t} + v \cdot \nabla G = s_{\mathrm{L,s}}|\nabla G| - D\kappa|\nabla G| \tag{6}$$

where $s_{\mathrm{L,s}} = s_{\mathrm{n}} + s_{\mathrm{r}}$, and s_{n} and s_{r} are contributions due to normal diffusion and reaction to the displacement speed of the thin reaction zone. However, $s_{\mathrm{L,s}}$ is the same order of magnitude as the laminar burning velocity. Therefore, the observed high turbulent burning velocities are accounted for by the $D\kappa$, in the second term on the right hand side of Eq. (6). It is conjectured that the magnitude of $D\kappa$ is much greater than the laminar burning velocity so that the modified G-equation would be able to represent premixed turbulent combustion in the thin reaction zones regime.

In 2009, Yuen and Gülder, using the same data presented in this work, evaluated the $D\kappa$ term. The value of the term $D\kappa$, the product of molecular diffusivity evaluated at reaction zone conditions and the flame front curvature, has been shown to be smaller than the magnitude of the laminar burning velocity. This finding questions the validity of extending the level set formulation, developed for corrugated flamelets region, into the thin reaction zones regime by modifying the local flame propagation by the term $D\kappa$.

One of the modeling approaches is to estimate the burning velocity from the integrated flame surface density or to use the modified level set equation. Our results question the validity of this approach and showed that beyond a certain nondimensional turbulence rms velocity, the surface growth of the flame front does not explain the observed burning rates. Also, the modified level set equation, Eq. (6), does not reflect the burning rates observed in the thin reaction zones regime (Yuen & Gülder, 2009).

CONCLUDING REMARKS

Premixed turbulent flames of methane-air stabilized on a Bunsen-type burner were studied to study the dynamics and structure of the flame front in a wide range of turbulence intensities. The flame front data were obtained using planar Rayleigh scattering, and particle image velocimetry was used to measure instantaneous velocity field for the experimental conditions studied. The fuel-air equivalence ratio range was from 0.6 to stoichiometric. The nondimensional turbulent rms velocity covered a range from 3 to 24.

Flame front thickness increased slightly with increasing nondimensional turbulence rms velocity. There was no significant difference in flame thickening whether the flame thickness was evaluated at progress variable values of 0.5 or 0.3. The probability density function of curvature showed a Gaussian-like distribution at all turbulence intensities in all sections of the flame.

Downloaded By: [Canadian Research Knowledge Network] At: 17:52 1 June 2010

In the nondimensional turbulence intensity range of up to 24, it was found that the maximum flame surface density and surface density profile as a function of the progress variable did not show any dependence on turbulence intensity. Also for the same flames, the integrated flame surface density was found to be insensitive to turbulence intensity.

Our findings imply that the conceptual increase in flame surface density by turbulence may not be the dominant mechanism for flame velocity enhancement in turbulent combustion in the region specified as the flamelet combustion regime by the current turbulent premixed combustion diagrams. Small-scale transport of heat and species may be more important and chemistry may not be decoupled from turbulence. Further, the applicability of the flamelet approach may be limited to a much smaller regime than presently believed.

Downloaded By: [Canadian Research Knowledge Network] At: 17:52 1 June 2010

ACKNOWLEDGEMENTS

The work reported in this paper was supported by a Collaborative Research Opportunities (NSERC-CRO) grant from Natural Sciences and Engineering Research Council of Canada. The authors would like to thank Dr. D. Pavé for the help with setting up the Rayleigh measurement system.

REFERENCES

Chen, Y.C., and Bilger, R.W. 2002. Experimental investigation of three-dimensional flame-front structure in premixed turbulent combustion-I: Hydrocarbon/air Bunsen flames. *Combust. Flame*, **131**, 400.

Chen, Y.-C. 2007. Measurement of flame front curvature based on Fourier transformation. *Combust. Theory Model.*, **11**, 333.

Cintosun, E., Smallwood, G.J., and Gülder, Ö.L. 2007. Flame surface fractal characteristics in premixed turbulent combustion at high turbulence intensities. *AIAA J.*, **45**, 2785.

de Goey, L.P.H., Plessing, T., Hermanns, R.T.E., and Peters, N. 2005. Analysis of flame thickness of turbulent flamelets in the thin-reaction zone regime. *Proc. Combust. Instit.*, **30**, 859.

Deschamps, B.M., Smallwood, G.J., Prieur, J., Snelling, D.R., and Gülder, Ö.L. 1996. Surface density measurements of turbulent premixed flames in a spark-ignition engine and a Bunsen-type burner using planar laser-induced fluorescence. *Proc. Combust. Instit.*, **26**, 427.

Dibble, R.W., and Hollenbach, R.E. 1981. Laser Rayleigh thermometry. *Proc. Combust. Instit.*, **18**, 1489.

Dinkelacker, F., Soika, A., Most, D., Hofmann, D., Leipertz, A., Polifke, W., and Dobbeling, K. 1998. Structure of locally quenched highly turbulent lean premixed flames. *Proc. Combust. Instit.*, **27**, 857.

Eckbreth, A.C. 1996. *Laser Diagnostics for Combustion Temperature and Diagnostics*, 2nd ed., Gordon and Breach Publishers, Kent, England, Chap. X.

Gülder, Ö.L. 2007. Contribution of small scale turbulence to burning velocity of flamelets in the thin reaction zone regime. *Proc. Combust. Instit.*, **31**, 1369.

Gülder, Ö.L., and Smallwood, G.J. 2007. Flame surface densities in premixed combustion at medium to high turbulence intensities. *Combust. Sci. Technol.*, **179**, 191.

Gülder, Ö.L., Smallwood, G.J., Wong, R., Snelling, D.R., Smith, R., Deschamps, B.M., and Sautet, J.C. 2000. Flame front surface characteristics in turbulent premixed propane/air combustion. *Combust. Flame*, **120**, 407.

Halter, F., Chauveau, C., Djedaili-Chaumeix, N., and Gökalp, I. 2005. Characterization of the effects of pressure and hydrogen concentration on laminar burning velocities of methane-hydrogen-air mixtures. *Proc. Combust. Instit.*, **30**, 201.

Haq, M.Z., Sheppard, C.G.W., Wooley, R., Greenhalgh, D.A., and Lockett, R.D. 2002. Wrinkling and curvature of laminar and turbulent premixed flames. *Combust. Flame*, **131**, 1.

Hartung, G., Hult, J., Kaminski, C.F., Rogerson, J.W., and Swaminathan, N. 2008. Effect of heat release on turbulence and scalar-turbulence interaction in premixed combustion. *Phys. Fluids*, **20**, 035110.

Kim, S.H., and Pitsch, H. 2007. Scalar gradient and small-scale structure in turbulent premixed combustion. *Phys. Fluids*, **19**, 115104.

Knaus, D.A., Sattler, S.S., and Gouldin, F.C. 2005. Three-dimensional temperature gradients in premixed turbulent flamelets via cross-plane Rayleigh imaging. *Combust. Flame*, **141**, 253.

Markstein, G.H. 1964. Theory of flame propagation. In Markstein, G. H. (Ed.) *Nonsteady Flame Propagation*, Pergamon Press, London, Chap. B, pp. 5–14.

Miles, R.B., Lempert, W.R., and Forkey, J.N. 2001. Laser Rayleigh scattering. *Measurement Sci. Technol.*, **12**, R33.

Moffat, H.K., and Goodwin, D. 2010. Cantera—An object-orientated software toolkit for chemical kinetics, thermodynamics, and transport processes. http://code.google.com/p/cantera (accessed on April 2010).

Peters, N. 2000. *Turbulent Combustion*. Cambridge University Press, Cambridge, England, Chap. 2, pp. 66–169.

Peters, N., Terhoeven, P., Chen, J.H., and Echekki, T. 1998. Statistics of flame displacement speeds from computations of 2-D unsteady methane-air flames. *Proc. Combust. Instit.*, **27**, 833.

Pope, S.B. 1988. The evolution of surfaces in turbulence. *Int. J. Eng. Sci.*, **26**, 445.

Shepherd, I.G. 1996. Flame surface density and burning rate in premixed turbulent flames. *Proc. Combust. Instit.*, **26**, 373.

Shepherd, I.G., and Ashurst, W.M.T. 1992. Flame front geometry in premixed turbulent flames. *Proc. Combust. Instit.*, **24**, 485.

Shepherd, I.G., Cheng, R.K., Plessing, T., Kortschik, C., and Peters, N. 2002. Premixed flame front structure in intense turbulence. *Proc. Combust. Instit.*, **29**, 1833.

Sinibaldi, J.O., Mueller, C.J., and Driscoll, J.F. 1998. Local flame propagation speeds along wrinkled, unsteady, stretched premixed flames. *Proc. Combust. Instit.*, **27**, 827.

Soika, A., Dinkelacker, F., and Leipertz, A. 1998. Measurement of the resolved flame structure of turbulent premixed flames with constant Reynolds number and varied stoichiometry. *Proc. Combust. Instit.*, **27**, 785.

Sutton, J.A., and Driscoll, J.F. 2004. Rayleigh scattering cross sections of combustion species at 266, 355 and 532 nm for thermometry applications. *Opt. Lett.*, **29**, 2620.

Wang, G.H., and Clemens, N.T. 2004. Effects of imaging system blur on measurements of flow scalars and scalar gradients. *Exp. Fluids*, **37**, 194.

Yuen, F.T.C. 2009. *Experimental Investigation of the Dynamics and Structure of Lean Premixed Turbulent Combustion*. Doctoral dissertation, University of Toronto, Institute for Aerospace Studies, Toronto, Canada.

Yuen, F.T.C., and Gülder, Ö.L. 2009. Premixed turbulent flame front structure investigation by Rayleigh scattering in the thin reaction zone regime. *Proc. Combust. Instit.*, **32**, 1747.

Downloaded By: [Canadian Research Knowledge Network] At: 17:52 1 June 2010